

Frequency-dependent conductivity of concentrated electrolytes: A stochastic density functional theory

Cite as: J. Chem. Phys. 161, 244501 (2024); doi: 10.1063/5.0236073

Submitted: 30 August 2024 • Accepted: 3 December 2024 •

Published Online: 23 December 2024



View Online



Export Citation



CrossMark

Haggai Bonneau,^{1,a)} Yael Avni,^{2,b)} David Andelman,^{1,c)} and Henri Orland^{3,d)}

AFFILIATIONS

¹School of Physics and Astronomy, Tel Aviv University, Ramat Aviv, 69978 Tel Aviv, Israel

²University of Chicago, James Franck Institute, 929 E 57th Street, Chicago, Illinois 60637, USA

³Institut de Physique Théorique, Université de Paris-Saclay, CEA, CNRS, F-91191 Gif-sur-Yvette Cedex, France

^{a)}haggai.bonneau@mail.huji.ac.il

^{b)}yavni@uchicago.edu

^{c)}Author to whom correspondence should be addressed: andelman@tauex.tau.ac.il

^{d)}henri.orland@ipht.fr

ABSTRACT

The response of ionic solutions to time-varying electric fields, quantified by a frequency-dependent conductivity, is essential in many electrochemical applications. Yet, it constitutes a challenging problem due to the combined effect of Coulombic interactions, hydrodynamics, and thermal fluctuations. Here, we study the frequency-dependent conductivity of ionic solutions using a stochastic density functional theory. In the limit of small concentrations, we recover the classical Debye and Falkenhagen (DF) result, predicting an increase in conductivity with field frequency. At higher concentrations, we use a modified Coulomb interaction potential that accounts for the hard-core repulsion between the ions, which was recently employed in the zero-frequency case. Consequently, we extend the DF result to concentrated electrolytes. We discuss experimental and numerical studies and the complexity of observing the DF effect in such setups.

© 2024 Author(s). All article content, except where otherwise noted, is licensed under a Creative Commons Attribution (CC BY) license (<https://creativecommons.org/licenses/by/4.0/>). <https://doi.org/10.1063/5.0236073>

I. INTRODUCTION

The transport properties of electrolyte solutions have been the subject of long-standing fundamental and applied research. Ion dynamics in a solvent is essential in many physical and chemical processes.^{1–4} Furthermore, diverse technological applications of ion transport range from electrochemical energy storage in batteries to the flow of ions and charged molecules through biological cell membranes (e.g., ion channels and pumps).^{5–10}

Debye and Hückel were the first to propose a theory of electrolytic conductivity that included ion–ion interactions.¹¹ Their approach involved the concept of an ionic cloud, wherein each ion is assumed to be surrounded by a smeared ionic distribution of a net opposite charge that gets distorted by the central ion's movement. A few years later, Onsager refined the Debye–Hückel theory to account consistently for central-ion diffusion. This resulted in the

century-old Debye–Hückel–Onsager (DHO) theory for DC (zero frequency) conductivity of electrolytes.^{12,13}

One of the earliest investigations into frequency-dependent conductivity was conducted by Debye and Falkenhagen (DF). The DF theory¹⁴ assumes a continuum solvent medium in the low-frequency limit. Moreover, the influence of ion–solvent interactions was not incorporated. The DF theory predicts that the real part of the conductivity increases with frequencies in the low-frequency limit.¹⁴ This result can be understood in the following way. The ionic cloud asymmetry exerts a drag force on the moving ion. This asymmetry is established over a timescale of the Debye time, $t_D \sim \lambda_D^2/D$, where λ_D is the Debye screening length and D is the ion diffusion constant. When an AC driving force with a period shorter than the Debye time is applied, the asymmetric shape of the ion cloud does not reach its maximum distortion (see Fig. 1). Hence, the drag force is reduced, and the conductivity increases.

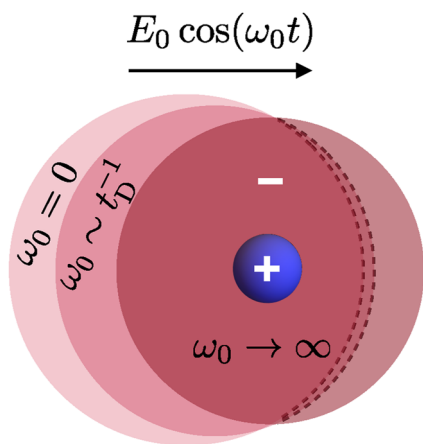


FIG. 1. Numerically obtained drawing of the negatively charged ionic cloud surrounding a cation in an electrolyte under an oscillatory external uniform electric field, $E_0 \cos(\omega_0 t)$, with amplitude E_0 and frequency ω_0 . The three superimposed red circles depict the distribution of the ionic cloud relative to the cation's position. Their shape is derived from the density–density correlation function between anions and cations [Eq. (32)], and it illustrates the cloud in its most distorted configuration over the oscillation period.

Conversely, a more recent analysis¹⁵ of the original experimental results by Falkenhagen¹⁶ has shown that the DF effect has never been adequately validated. The challenge in observing this effect is that its magnitude is relatively small, and the model can be justified only at very low concentrations. More recently, calculations have been carried out for the conductivity at higher concentrations using the *mode-coupling theory*, incorporating relaxation of the ionic cloud and hydrodynamic effects.^{17–21} These investigations describe the coupling between a tagged ion and the collective slow-mode dynamics in terms of several self-consistent equations. It allows a numerical (but not closed-form expressions) evaluation of the conductivity in various cases, including high-concentration and time-dependent external fields.

Advances in nonequilibrium statistical mechanics included the formulation of the *stochastic density functional theory* (SDFT)^{22,23} and led to a different approach to calculating the ionic conductivity in the dilute limit.^{24,25} The governing equation in this approach is often called the Kawasaki–Dean equation and does not rely on an ionic cloud or coupling to the system's collective variables. Instead, SDFT accounts for the microscopic ion–ion interactions and allows a systematic derivation of macroscopic quantities in the dilute regime.

Quite recently, SDFT has been employed^{26,27} with a modified interaction potential between the ions, taking into account the short-range steric interaction. This modified electrostatic potential allowed a better treatment than DHO at a higher concentration range, in which the ions, on average, are much closer to one another. The theory successfully predicted the conductivity of NaCl solutions (and other monovalent salts) up to a few molars without any fit parameters; the DHO theory fails above 10 mM. Moreover, this framework and the modified potential were used to predict viscosity corrections in concentrated electrolytes.²⁸ However, other studies²⁹

emphasize that despite the advantages of SDFT coupled with a modified potential, it should be handled with caution above a few hundred millimolars.

In separate studies, several dynamic aspects of electrolytes have been investigated using SDFT.^{30,31} It was found that the current response of an electrolyte to a quench of the electric field from finite values to zero is rather complex. The main finding is a non-monotonic response followed by an algebraic relaxation of the conductivity as a function of time.

In this study, we employ SDFT to compute the frequency-dependent conductivity of binary monovalent electrolytes. We present the conductivity as a function of the interaction potential between the same and oppositely charged ions. We follow Refs. 26 and 27 and consider similarly the modified ion–ion interaction potential that takes into account approximately the ionic hard-core repulsion. Using such modified potential, we compute a closed-form expression for the electrolyte conductivity at finite frequencies of an AC external electric field and for an extensive range of concentrations. We show that our theory reduces to the DF one without short-range steric interactions. Finally, we show that our theory is relatively robust to different choices of short-range repulsion.

The outline of this paper is as follows. In Sec. II, we present the model and derive the general expressions for the conductivity of an ionic solution with an arbitrary number of species for any interaction potential and time-dependent applied field. In Sec. III, we focus on binary electrolytes and derive the frequency-dependent conductivity for different interaction potentials under the weak amplitude limit of the electric field. In Sec. IV, we discuss our results and their connection to experiments and simulations. Finally, in Sec. V, we conclude and suggest future experiments to test our predictions.

II. MODEL

A. Equations of motion

We consider a system composed of a continuous and homogeneous solvent (e.g., water) with a dielectric constant $\epsilon = \epsilon_r \epsilon_0$, where ϵ_0 is the vacuum permittivity in SI units and ϵ_r is the relative (dimensionless) dielectric constant. Besides the dielectric constant, the solvent is characterized by its viscosity η , and the system is kept at temperature T . Cations and anions are modeled as charged Brownian particles, solubilized in a three-dimensional fluid, forming an electrolyte solution. The system is then subjected to a time-dependent external electric field that is uniform in space and of the form $\mathbf{E}(t) = E_0 g(t) \hat{\mathbf{x}}$, where $\hat{\mathbf{x}}$ is the unit vector along the x axis and E_0 is the electric field amplitude. The function $g(t)$ is a dimensionless function of order unity that encodes the time dependence of the external electric field and has a Fourier transform $\hat{g}(\omega)$.

Each ionic species $\alpha = 1, \dots, M$, has a charge $z_\alpha e$, where z_α is the valency and e is the electronic unit charge, and its bulk number density is n_α^0 . The external field induces a charge current density, $J(E)$, along the same direction as the external field \mathbf{E} . Finally, the DC conductivity is defined by the ratio

$$\kappa = \frac{J(E)}{E_0} \Big|_{E_0=0} \quad \text{with } g(t) = 1. \quad (1)$$

At infinite dilution ($n_\alpha^0 \rightarrow 0$) and constant external field $E = E_0 \hat{x}$, the ions perform a Brownian motion with a mean velocity of $e z_\alpha \mu_\alpha E_0$ along the field direction, where μ_α is the ion mobility related to D_α by the Einstein relation $\mu_\alpha = D_\alpha / k_B T$, and k_B is the Boltzmann constant. The conductivity κ_0 in the infinite dilution limit $n_\alpha^0 \rightarrow 0$ is called the Nernst–Einstein conductivity and is given by $\kappa_0 = e^2 \sum_\alpha z_\alpha^2 \mu_\alpha n_\alpha^0$.

At low ionic densities, the interactions between the ions reduce the conductivity. The zero-frequency correction to κ_0 , to leading order in n_α^0 , is given by the DHO result.¹² For a binary monovalent electrolyte, it is given as

$$\kappa(\omega = 0) = \kappa_0 \left[1 - \frac{r_s}{\lambda_D} - \frac{1}{3} \left(1 - \frac{1}{\sqrt{2}} \right) \frac{l_B}{\lambda_D} \right], \quad (2)$$

where $r_s = (6\pi\eta\mu)^{-1}$ is the Stokes' hydrodynamic radius of charged particles, in which

$$\lambda_D = \sqrt{\epsilon k_B T / 2n_\alpha^0 e^2}, \quad (3)$$

is the Debye length, and $l_B = e^2 / (4\pi\epsilon k_B T)$ is the Bjerrum length. At room temperature in water, $l_B \approx 7 \text{ \AA}$. In the dilute limit, the characteristic length for which the electrostatic interactions are screened is the Debye length, λ_D . Together with the diffusion coefficient averaged over the species types, \bar{D} , a time scale (called the Debye time) can be constructed,

$$t_D = \lambda_D^2 / \bar{D}, \quad (4)$$

and it describes the characteristic relaxation time of the ionic cloud.

Similar to the definition of the DC conductivity in Eq. (1), the frequency-dependent conductivity is defined as

$$\kappa(\omega) = \frac{\hat{J}(\omega, E)}{E_0 \hat{g}(\omega)} \Big|_{E_0=0}, \quad (5)$$

where $\hat{J}(\omega, E)$ is the Fourier transform of $J(t, E)$.

In the following, we study the dynamics of the number density current \mathbf{j}_α of the ionic species α . These currents are related to the total average ionic current by

$$\mathbf{J} = e \sum_{\alpha=1}^M z_\alpha \langle \mathbf{j}_\alpha \rangle, \quad (6)$$

where $\langle \dots \rangle$ is a thermal average over the fluctuations. We proceed by describing the temporal evolution of the ionic density field $n_\alpha(\mathbf{r}, t)$ of the species α using SDFT^{22,24} that also includes the hydrodynamic interactions,^{25,27,32}

$$\frac{\partial n_\alpha}{\partial t} = -\nabla \cdot \mathbf{j}_\alpha, \quad (7)$$

$$\mathbf{j}_\alpha = n_\alpha \mathbf{u} - D_\alpha \nabla n_\alpha + \mu_\alpha \mathbf{f}_\alpha + \sqrt{2D_\alpha n_\alpha} \boldsymbol{\zeta}_\alpha.$$

The first equation is the continuity equation, while the second describes the fluctuating dynamics of the ionic number current density, \mathbf{j}_α . The first and second terms of \mathbf{j}_α in Eq. (7) are the advection and diffusion terms, respectively, where $\mathbf{u}(\mathbf{r}, t)$ is the solvent velocity field. The third term accounts for the motion due to the external

field and inter-ionic forces, where $\mathbf{f}_\alpha(\mathbf{r}, t)$ is the force density acting on the α species particles. Finally, the fourth term in Eq. (7) is a stochastic field, where $\boldsymbol{\zeta}(\mathbf{r}, t)$ is a three-dimensional Gaussian white noise satisfying

$$\langle \boldsymbol{\zeta}_\alpha(\mathbf{r}, t) \rangle = 0, \quad (8)$$

$$\langle \zeta_\alpha^n(\mathbf{r}, t) \zeta_\beta^m(\mathbf{r}', t') \rangle = \delta_{\alpha\beta} \delta_{nm} \delta(\mathbf{r} - \mathbf{r}') \delta(t - t'),$$

where ζ_α^n and ζ_α^m denote the n th and m th Cartesian coordinates of the vector $\boldsymbol{\zeta}_\alpha$, respectively, δ_{ij} is the Kronecker delta function, and the δ -function is the Dirac delta function in the appropriate dimension. Throughout this paper, we use the Itô convention^{22,33} for the multiplicative noise [as in Eq. (7)].

The force density \mathbf{f}_α is the sum of the forces exerted by the external field and the force density due to pair interactions with other ions,

$$\mathbf{f}_\alpha = n_\alpha z_\alpha e \mathbf{E} - n_\alpha \sum_{\beta=1}^M \nabla V_{\alpha\beta} * n_\beta, \quad (9)$$

where $V_{\alpha\beta}(\mathbf{r})$ is the interaction potential between the α and β species, and the symbol “*” denotes the convolution operator, $h * g \equiv \int d^3 r' h(\mathbf{r}') g(\mathbf{r} - \mathbf{r}')$.

The small ionic size typically results in a very low Reynolds number, meaning that hydrodynamic effects in electrolyte systems are adequately described by the incompressible laminar flow.¹² Therefore, we assume that the fluid velocity field $\mathbf{u}(\mathbf{r}, t)$ satisfies the Stokes' equation for incompressible fluids,

$$\nabla \cdot \mathbf{u} = 0, \quad (10)$$

$$\eta \nabla^2 \mathbf{u} - \nabla p = -\sum_\alpha \mathbf{f}_\alpha,$$

where p is the fluid pressure field.

As we focus hereafter on the frequency-dependent response, our approach neglects inertial effects corresponding to the relaxation of the ion velocity. This occurs on a time scale $t_I = m_{\text{ion}} D / k_B T$, with m_{ion} being the ion mass. For frequencies larger than $1/t_I \sim 10^{13} \text{ s}^{-1} = 10 \text{ THz}$, the overdamped dynamics description is insufficient. Instead, it would be necessary to consider the full Newtonian description of the ions and the solvent, as in the Navier–Stokes equation. In addition, our model neglects the frequency dependence of the solvent permittivity. This dependence significantly reduces the permittivity for frequencies larger than 10 GHz.^{35,36} Note that we discard the noise term in the Stokes' equation, as this term is divergence-free and will not affect the species density n_α (see, e.g., Ref. 31 for further discussion).

We can integrate over the solvent degrees of freedom $\mathbf{u}(\mathbf{r})$ to obtain a closed-form expression for the current densities, \mathbf{j}_α . The solution for Eq. (10) is given by³⁴

$$\mathbf{u} = \sum_\beta \mathcal{O} * \mathbf{f}_\beta, \quad (11)$$

and

$$\mathcal{O}_{ij}(\mathbf{r}) = \frac{1}{8\pi\eta} \left(\frac{\delta_{ij}}{r} + \frac{r_i r_j}{r^3} \right), \quad i, j = 1, 2, 3. \quad (12)$$

Substituting this result in the expression for the density current, Eq. (7), we get

$$\mathbf{j}_\alpha = -D_\alpha \nabla n_\alpha + \mu_\alpha \mathbf{f}_\alpha + n_\alpha \sum_\beta \mathcal{O} * \mathbf{f}_\beta + \sqrt{2D_\alpha n_\alpha} \zeta_\alpha. \quad (13)$$

B. Conductivity calculation

Substituting Eq. (13) in Eq. (6) leads to

$$\mathbf{J} = \kappa_0 \mathbf{E} - \sum_{\alpha, \beta} e z_\alpha \mu_\alpha \langle n_\alpha \nabla V_{\alpha\beta} * n_\beta \rangle + \sum_{\alpha, \beta} e^2 z_\alpha z_\beta \langle n_\alpha \mathcal{O} * n_\beta \rangle \mathbf{E}. \quad (14)$$

Note that the stochastic (noise) term in Eq. (13) cancels as it is uncorrelated with the density fields at time t . Moreover, the gradient term cancels as the system is assumed to be homogeneous on average. Finally, a term that is third order in the concentration is discarded as it does not contribute to the linearized theory (see Ref. 31 for further discussion).

Now, we introduce the density fluctuation $\delta n_\alpha(\mathbf{r}, t)$ for each α species,

$$\delta n_\alpha(\mathbf{r}, t) = n_\alpha(\mathbf{r}, t) - n_\alpha^0, \quad (15)$$

and express the average ionic current \mathbf{J} as a function of the density–density correlation, which is given by

$$C_{\alpha\beta}(\mathbf{r} - \mathbf{r}', t) \equiv \langle \delta n_\alpha(\mathbf{r}, t) \delta n_\beta(\mathbf{r}', t) \rangle. \quad (16)$$

Writing the convolution explicitly and using the correlation as defined in Eq. (16), we find

$$\begin{aligned} \mathbf{J} = & \kappa_0 \mathbf{E} - \sum_{\alpha, \beta} e z_\alpha \mu_\alpha \int d^3 r \nabla V_{\alpha\beta}(\mathbf{r}) C_{\alpha\beta}(\mathbf{r}, t) \\ & + \sum_{\alpha, \beta} e^2 z_\alpha z_\beta \mathbf{E} \int d^3 r \mathcal{O}(\mathbf{r}) C_{\alpha\beta}(\mathbf{r}, t). \end{aligned} \quad (17)$$

The correction to the bare current, $\kappa_0 \mathbf{E}$, is the sum of two contributions. The first term involves the electrostatic potential $V_{\alpha\beta}$ and is referred to as the *electrostatic correction* (also known as the relaxation correction). It represents the deformation of the counterion cloud around each of the ions by the external electric field. The second term involves the Oseen tensor \mathcal{O} and the external field \mathbf{E} . It is called the *hydrodynamic correction* (also known as the electrophoretic correction). It contains the effect of the flow created by the counterion cloud under the action of the external field.

The diagonal part of the correlation matrix contains the self-interaction term related to the diffusion constant. Our theory treats diffusion and hydrodynamic interaction separately, so, to compute the hydrodynamic correction correctly, it is necessary to subtract the self-interaction. This is performed by substituting

$$C_{\alpha\beta}(\mathbf{r} - \mathbf{r}', t) \rightarrow C_{\alpha\beta}(\mathbf{r} - \mathbf{r}', t) - n_\alpha^0 \delta_{\alpha\beta} \delta(\mathbf{r} - \mathbf{r}'). \quad (18)$$

We remark that this modified correlation does not affect the electrostatic correction.

Using Parseval's theorem, we express the above-mentioned equation in Fourier space and obtain

$$\begin{aligned} \mathbf{J}(t) = & \kappa_0 \mathbf{E}(t) + \sum_{\alpha, \beta} e z_\alpha \mu_\alpha \int \frac{d^3 k}{(2\pi)^3} (i\mathbf{k}) \tilde{V}_{\alpha\beta}(\mathbf{k}) \tilde{C}_{\alpha\beta}(\mathbf{k}, t) \\ & + \sum_{\alpha, \beta} e^2 z_\alpha z_\beta \mathbf{E}(t) \int \frac{d^3 k}{(2\pi)^3} \tilde{\mathcal{O}}(\mathbf{k}) \tilde{C}_{\alpha\beta}(\mathbf{k}, t), \end{aligned} \quad (19)$$

where we denote the spatial Fourier transform of $h(\mathbf{r})$ as $\tilde{h}(\mathbf{k}) \equiv \int d^3 r h(\mathbf{r}) e^{-i\mathbf{k}\cdot\mathbf{r}}$. Note that the Fourier transform of the interaction potential and the Oseen tensor is even in \mathbf{k} , $\tilde{V}_{\alpha\beta}(\mathbf{k}) = \tilde{V}_{\alpha\beta}(-\mathbf{k})$ and $\tilde{\mathcal{O}}(\mathbf{k}) = \tilde{\mathcal{O}}(-\mathbf{k})$.

As we are interested in the frequency-dependent conductivity, we perform an additional Fourier transform from the time domain, t , into the frequency domain, ω ,

$$\begin{aligned} \tilde{\mathbf{J}}(\omega) = & \kappa_0 \tilde{\mathbf{E}}(\omega) + \sum_{\alpha, \beta} e z_\alpha \mu_\alpha \int \frac{d^3 k}{(2\pi)^3} (i\mathbf{k}) \tilde{V}_{\alpha\beta}(\mathbf{k}) \tilde{C}_{\alpha\beta}(\mathbf{k}, \omega) \\ & + \sum_{\alpha, \beta} e^2 z_\alpha z_\beta \int \frac{d^3 k}{(2\pi)^3} \int d\omega' \tilde{\mathcal{O}}(\mathbf{k}) \tilde{C}_{\alpha\beta}(\mathbf{k}, \omega') \tilde{\mathbf{E}}(\omega - \omega'), \end{aligned} \quad (20)$$

where the spatio-temporal Fourier transform of a function $h(\mathbf{r}, t)$ is denoted as $\tilde{h}(\mathbf{k}, \omega) \equiv \int d^3 r dt h(\mathbf{r}, t) e^{-i\mathbf{k}\cdot\mathbf{r} - i\omega t}$. Equation. (20) is the general expression for the Fourier transform of the current $\tilde{\mathbf{J}}(\omega)$ expressed in terms of the Fourier transform of any two-body potential $\tilde{V}_{\alpha\beta}(\mathbf{k})$, external electric field $\tilde{\mathbf{E}}(\omega)$, and density–density correlations $\tilde{C}_{\alpha\beta}(\mathbf{k}, \omega)$. Finally, note that in our study, \mathbf{J} and \mathbf{E} are homogeneous temporal functions in space.

C. Linearized SDFT

To get more straightforward analytical results, we return to Eq. (13) in position space and linearize it around the ionic bulk densities, n_α^0 . The resulting evolution equation for the ionic density fluctuations of the α species, $\delta n_\alpha = n_\alpha - n_\alpha^0$, reads

$$\begin{aligned} \frac{\partial}{\partial t} \delta n_\alpha = & D_\alpha \nabla^2 \delta n_\alpha - \mu_\alpha e z_\alpha \mathbf{E}(t) \cdot \nabla \delta n_\alpha + \mu_\alpha n_\alpha^0 \nabla^2 \left[\sum_\beta V_{\alpha\beta} * \delta n_\beta \right] \\ & + \sqrt{2D_\alpha n_\alpha^0} \nabla \cdot \zeta_\alpha. \end{aligned} \quad (21)$$

The dynamic equation can be written in a simplified form in the Fourier k -space,

$$\frac{d}{dt} \delta \tilde{n}_\alpha = -A_{\alpha\beta} \delta \tilde{n}_\beta + \chi_\alpha, \quad (22)$$

where the matrix \mathbf{A} is given by

$$A_{\alpha\beta}(\mathbf{k}, t) = \delta_{\alpha\beta} [D_\alpha k^2 + i\mu_\alpha e z_\alpha \mathbf{E}(t) \cdot \mathbf{k}] + \mu_\alpha n_\alpha^0 k^2 \tilde{V}_{\alpha\beta}. \quad (23)$$

We also introduced a scalar Gaussian noise $\chi_\alpha(\mathbf{k}, t)$ that satisfies

$$\langle \chi_\alpha(\mathbf{k}, t) \chi_\beta(\mathbf{k}', t') \rangle = 2(2\pi)^3 B_{\alpha\beta} \delta(\mathbf{k} + \mathbf{k}') \delta(t - t'), \quad (24)$$

with a diagonal noise correlation matrix $B_{\alpha\beta} = \delta_{\alpha\beta} n_\alpha^0 D_\alpha k^2$. Hence, in Fourier space, the density–density correlations are given by

$$\langle \delta \tilde{n}_\alpha(\mathbf{k}, t) \delta \tilde{n}_\beta(\mathbf{k}', t) \rangle = (2\pi)^3 \delta(\mathbf{k} + \mathbf{k}') \tilde{C}_{\alpha\beta}(\mathbf{k}, t). \quad (25)$$

Using the Itô product rule (see Secs. 4.3 and 4.4 of Ref. 37) in Eq. (22), we find that the correlation matrix \tilde{C} satisfies

$$\frac{d}{dt}\tilde{C} = 2\mathbf{B} - \mathbf{A}\tilde{C} - \tilde{C}\mathbf{A}^*, \quad (26)$$

where the matrix \mathbf{A}^* is the complex conjugate of \mathbf{A} . Equation (26) is a set of linear inhomogeneous (with a source) and non-autonomous (with an explicit dependence on the time variable t) first-order ordinary differential equations (ODEs). In Sec. III, we consider binary monovalent electrolytes for which Eq. (26) can be further simplified.

III. RESULTS

A. Binary monovalent electrolyte

For binary monovalent 1:1 electrolytes (such as table salt, NaCl), the electrolyte comprises cation–anion pairs, $\alpha = \pm$, with charges $z_{\pm}e = \pm e$. Because of the overall charge neutrality, $n_{\pm}^0 = n_0$, we further assume that the ionic mobilities are the same, $\mu_{\pm} = \mu$, implying $D_{\pm} = D$.

Using the symmetry of the 1:1 electrolytes, we know that $\tilde{C}_{--} = \tilde{C}_{++}$ and $\tilde{C}_{+-} = \tilde{C}_{-+}^*$. Hence, the elements of the 2×2 correlation matrix can be expressed via three independent functions: \tilde{c} , \tilde{r} , and \tilde{m} , where

$$\begin{aligned} \tilde{c}(\mathbf{k}, \omega) &\equiv \frac{1}{n_0}\tilde{C}_{++}(\mathbf{k}, \omega), \\ \tilde{r}(\mathbf{k}, \omega) &\equiv \frac{1}{n_0}\text{Re}[\tilde{C}_{+-}(\mathbf{k}, \omega)], \\ \tilde{m}(\mathbf{k}, \omega) &\equiv \frac{1}{n_0}\text{Im}[\tilde{C}_{+-}(\mathbf{k}, \omega)]. \end{aligned} \quad (27)$$

We then choose the following form of the modified electrostatic potential in k -space: $\tilde{V}_{\alpha\beta} = (e^2/\epsilon)v_{\alpha\beta}(k, a)$, where $k \equiv |\mathbf{k}|$ and a is a length scale related to the short-range repulsion between the ions. The behavior of $v_{\alpha\beta}$ at $ka \ll 1$ recovers the standard Coulomb potential, $\sim 1/k^2$, but deviates when $ka \approx 1$, where its functional form depends on a .

It is convenient to introduce dimensionless variables. The spatial coordinates are rescaled by the Debye length so that $\mathbf{q} \equiv \mathbf{k}\lambda_D$, while time and frequency are rescaled by the Debye time so that $\Omega \equiv \omega t_D$ and $\tau \equiv t/t_D$. Applying these dimensionless variables, the integrals in Eq. (20) are rewritten in a dimensionless form. By dividing $\tilde{J}(\Omega, E)$ by $\tilde{g}(\Omega)E_0$, one gets the frequency-dependent conductivity,

$$\frac{\tilde{J}(\Omega, E)}{\tilde{g}(\Omega)E_0} = \kappa_0 + \kappa_{\text{el}}(\Omega) + \kappa_{\text{hyd}}(\Omega), \quad (28)$$

where the electrostatic and hydrodynamic corrections read

$$\begin{aligned} \kappa_{\text{el}}(\Omega, \mathcal{E}) &= -\frac{\kappa_0}{2\pi^2} \frac{l_B}{\lambda_D} \frac{1}{\tilde{g}(\Omega)} \mathcal{E} \int d^3q q_x \tilde{m}(\Omega, q) v_{+-}(q), \\ \kappa_{\text{hyd}}(\Omega, \mathcal{E}) &= \frac{3\kappa_0}{4\pi^2} \frac{r_s}{\lambda_D} \frac{1}{\tilde{g}(\Omega)} \int d\Omega' \int \frac{d^3q}{q^2} (1 - q_x^2/q^2) \\ &\quad \times [\tilde{c}(\Omega', q) - \tilde{r}(\Omega', q) - \delta(\Omega')] \tilde{g}(\Omega - \Omega'), \end{aligned} \quad (29)$$

respectively, where $\mathcal{E} \equiv e\lambda_D E_0/k_B T$ is the dimensionless electric field. Using the same rescaling, we can write the SDFT equation for the correlation functions as

$$\begin{aligned} \frac{d\tilde{c}}{d\tau} &= -q^2(2 + v_{++})\tilde{c}(\tau) - q^2 v_{-+}\tilde{r}(\tau) + 2q^2, \\ \frac{d\tilde{r}}{d\tau} &= -q^2(2 + v_{++})\tilde{r}(\tau) - q^2 v_{-+}\tilde{c}(\tau) + 2\mathcal{E}q_x g(\tau)\tilde{m}(\tau), \\ \frac{d\tilde{m}}{d\tau} &= -q^2(2 + v_{++})\tilde{m}(\tau) - 2\mathcal{E}q_x g(\tau)\tilde{r}(\tau). \end{aligned} \quad (30)$$

Finding a general closed-form solution to the set of Eq. (30) is difficult. Hence, we look for periodic solutions in the small electric field \mathcal{E} limit. To do so, we examine the temporal Fourier transform of Eq. (30),

$$\begin{aligned} \tilde{c}(\Omega) &= \frac{2q^2\delta(\Omega) - q^2 v_{-+}\tilde{r}(\Omega)}{\Lambda(\Omega)}, \\ \tilde{r}(\Omega) &= \frac{2\mathcal{E}q_x(\tilde{m} * \tilde{g})(\Omega) - q^2 v_{-+}\tilde{c}(\Omega)}{\Lambda(\Omega)}, \\ \tilde{m}(\Omega) &= -\frac{2\mathcal{E}q_x(\tilde{r} * \tilde{g})(\Omega)}{\Lambda(\Omega)}, \end{aligned} \quad (31)$$

where $\Lambda(\Omega) = i\Omega + q^2(2 + v_{++})$.

Solving these equations that give the system's limit cycle is not straightforward. Yet, one can solve them to the leading order in \mathcal{E} and get the frequency-dependent conductivity computed at vanishing electric fields as

$$\begin{aligned} \tilde{c}^{(0)}(\Omega) &= \frac{4 + 2v_{++}}{(2 + v_{++})^2 - v_{-+}^2} \delta(\Omega), \\ \tilde{r}^{(0)}(\Omega) &= -\frac{2v_{-+}}{(2 + v_{++})^2 - v_{-+}^2} \delta(\Omega), \\ \tilde{m}^{(1)}(\Omega) &= \frac{4q_x v_{-+} \tilde{g}(\Omega)}{[(2 + v_{++})^2 - v_{-+}^2][i\Omega + q^2(2 + v_{++})]}, \end{aligned} \quad (32)$$

where the superscript (i) denotes the i th term in the power expansion of \mathcal{E} . Note that the terms $\tilde{m}^{(0)}$, $\tilde{c}^{(1)}$, and $\tilde{r}^{(1)}$ are equal to zero and are discarded. In Fig. 2, the real-space and time-dependent correlation function $c_{+-}(x/\lambda_D, y/\lambda_D, t)$ is computed for Coulombic interactions and with $g(t) = \cos(\omega_0 t)$.

Expressing the integrals in Eq. (29) using Eq. (32) yields

$$\begin{aligned} \kappa_{\text{el}}(\Omega) &= -\frac{8\kappa_0}{3\pi} \frac{l_B}{\lambda_D} \int_0^\infty dq \\ &\quad \times \frac{q^4 v_{-+}^2}{[(2 + v_{++})^2 - v_{-+}^2][q^2(2 + v_{++}) + i\Omega]}, \\ \kappa_{\text{hyd}} &= -\frac{2\kappa_0}{\pi} \frac{r_s}{\lambda_D} \int_0^\infty dq \frac{v_{++} - v_{-+}}{2 + v_{++} - v_{-+}}. \end{aligned} \quad (33)$$

Equation (33) gives the frequency-dependent conductivity for a binary monovalent electrolyte as a function of the interaction potential between the ions.

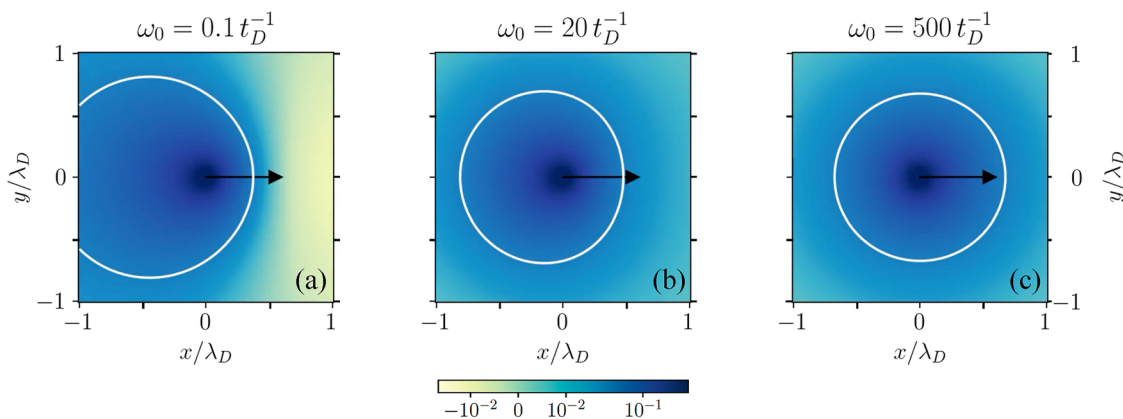


FIG. 2. Density–density correlation function $c_{+-}(x/\lambda_D, y/\lambda_D, t)$, where the lengths are measured in units of λ_D . The correlation c_{+-} is computed by taking numerically the Fourier transform of the solution in Eq. (32), for $g(t) = \cos(\omega_0 t)$. A pure Coulomb interaction potential is used. The three panels show a colormap of c_{+-} at $t = 0$ (when the electric field magnitude is at its maximum) for different values of ω_0 . In order to enhance the figure’s deformation visibility, we set $\mathcal{E} = 3$. The arrows indicate the direction of the electric field. The oscillation in panel (a) is slow compared to t_D . Therefore, the correlation shape reaches a strongly asymmetric form along the direction of the electric field. Panel (c) shows the opposite case, when the field oscillation is fast compared to t_D , leading to an almost spherically symmetric correlation. Panel (b) shows an intermediate case. See the [supplementary material](#) for an animation of the correlation function evolution over time.

B. Pure Coulomb potential

Evaluating the integrals in Eq. (33) for Coulomb potential, namely

$$v_{++} = -v_{+-} = 1/k^2, \quad (34)$$

recovers the well-known Debye–Falkenhagen (DF) result,¹⁴

$$\kappa_{\text{el}}(\omega) = -\frac{\kappa_0 l_B}{3 \lambda_D} \frac{1}{2 + \sqrt{2 + 2i\omega t_D}}, \quad (35)$$

where the DF result is expressed in terms of the physical frequency, $\omega = \Omega t_D$. Examining Eqs. (29) and (32), we see that the hydrodynamic correction depends on the zeroth order terms in \mathcal{E} of the correlations. Therefore, it is independent of ω ,

$$\kappa_{\text{hyd}} = -\kappa_0 \frac{r_s}{\lambda_D}. \quad (36)$$

We can also see that the standard DHO correction is recovered at the $\omega \rightarrow 0$ limit [Eq. (2)]. Similar to the DHO result, Eqs. (35) and (36) are limited to small concentrations, typically lower than 10 mM.

C. Modified potentials

The original DF result can be improved by introducing an interaction potential that accounts for the repulsion between the ions at short ranges.

An effective potential that takes into account the steric interaction should contain the scale for which the steric repulsion between ions becomes substantial, namely, when the distance between the two particle centers is equal to the sum of their radii, $r_\alpha + r_\beta$. For simplicity, we define a as such a characteristic length, ignoring the size difference between ions of different species.

The truncated Coulomb potential has been previously proposed to account for the short-range interaction between ions.^{26,27,38} It is written as

$$V_{\alpha\beta}(r) = \frac{e^2 z_\alpha z_\beta}{4\pi\epsilon} \frac{\theta(r-a)}{r}, \quad (37)$$

where θ is the Heaviside function. Using the truncated potential in Eq. (33) gives the following expressions for the two conductivity correction terms:

$$\begin{aligned} \kappa_{\text{el}}(\omega) &= -\frac{2\kappa_0 l_B}{3\pi \lambda_D} \int_0^\infty dq \frac{q^2 \cos^2\left(\frac{aq}{\lambda_D}\right)}{\left[\cos\left(\frac{aq}{\lambda_D}\right) + q^2\right] \left[\cos\left(\frac{aq}{\lambda_D}\right) + 2q^2 + i\omega t_D\right]}, \\ \kappa_{\text{hyd}} &= -\frac{2\kappa_0 r_s}{\pi \lambda_D} \int_0^\infty dq \frac{\cos\left(\frac{aq}{\lambda_D}\right)}{\cos\left(\frac{aq}{\lambda_D}\right) + q^2}. \end{aligned} \quad (38)$$

We recall that the truncated potential is a useful approximation for the interaction between ions in an electrolyte as it takes into account the finite ionic size, but it comes with certain drawbacks. The two terms in Eq. (38) diverge at high concentrations even for DC fields ($\omega = 0$). This divergence occurs when the term $[\cos(aq/\lambda_D) + q^2]$ in the denominator crosses zero. For large concentrations, a/λ_D that scales as $n^{1/2}$ becomes large so that the cosine term becomes negative while $q \leq 1$, leading to the divergence of the integral.

Moreover, while the total conductivity was shown²⁷ to agree well with experimental results up to 3M, a recent comparison of each contribution to Brownian dynamic simulations suggested that each term by itself (κ_{el} and κ_{hyd}) is unreliable at high concentrations (roughly above 1M). Therefore, our results are presented only for concentrations up to 1M. See Refs. 26 and 29 for more details.

Another modified potential is a soft truncated potential that was proposed in Refs. 39–41,

$$V_{\alpha\beta}(r) = \frac{e^2 z_\alpha z_\beta}{4\pi\epsilon} \left(\frac{1}{r} - \frac{e^{-r/a}}{r} \right). \quad (39)$$

This potential gives simpler polynomial expressions in Fourier space that can be integrated exactly. However, the exact expressions are rather elaborate and will not be presented here. Substituting Eq. (39) in Eq. (33), we get

$$\kappa_{\text{el}}(\omega) = -\frac{2\kappa_0}{3\pi} \frac{l_B}{\lambda_D} \int_0^\infty dq \frac{q^2}{\left[\left(\frac{a}{\lambda_D} \right)^2 q^4 + q^2 + 1 \right]} \times \frac{1}{\left[2 \left(\frac{a}{\lambda_D} \right)^2 q^4 + q^2 \left(2 + i \frac{a^2}{\lambda_D^2} \omega \right) + i \omega t_D + 1 \right]}, \quad (40)$$

$$\kappa_{\text{hyd}} = -\kappa_0 \frac{r_s}{\lambda_D} \frac{1}{\sqrt{1 + 2a/\lambda_D}}.$$

Unlike the truncated potential, the soft truncated potential does not produce the divergence of the two correction terms at high concentrations. However, for concentrations below 1M, the two potentials give very similar results.

IV. DISCUSSION

By examining Eq. (33), we can see that the electrostatic correction κ_{el} depends on the external-field frequency ω . In contrast, the hydrodynamic correction κ_{hyd} remains the same as in the stationary case. In Fig. 3, we compare the numerical evaluations of $\kappa(\omega)$ [Eq. (28)] with the three different potentials: Coulomb, truncated Coulomb, and soft truncated Coulomb.

For simple ions in aqueous solutions at room temperature, the parameter values used are $l_B = 7 \text{ \AA}$, $\lambda_D = 3 \text{ \AA} / \sqrt{n[\text{M}]}$, $r_s = 1.5 \text{ \AA}$, and $a = 3 \text{ \AA}$. The Debye time has a typical value of $t_D = (10^{-10}/n[\text{M}]) \text{ s}$. One can see that the conductivity increase starts when $\omega t_D \approx 1$. The truncated and soft truncated Coulomb potentials give roughly the same conductivity for $a \approx \lambda_D$ at moderate frequencies. Different choices of potentials affect the correction to the conductivity at driving frequencies that exceed $\omega t_D \gtrsim 1000$. However, within this range of very high frequencies, our model does not hold as it is based on overdamped dynamics.

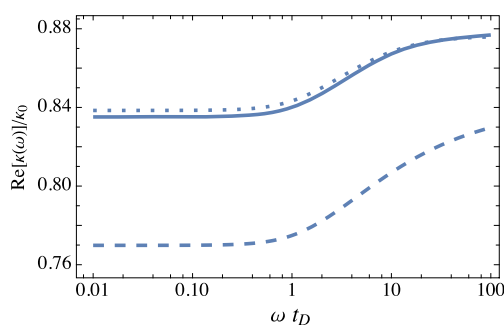


FIG. 3. Real part of the normalized conductivity as a function of ωt_D for the three interaction potentials. The Coulomb potential [Eqs. (35) and (36)] is plotted with a dashed line, the truncated potential [Eq. (38)] with a solid line, and the soft-truncated potential [Eq. (40)] with a dotted line. The solution concentration is taken as $n = 0.1\text{M}$. The other parameter values are $l_B = 7 \text{ \AA}$, $\lambda_D = 10 \text{ \AA}$, $r_s = 1.5 \text{ \AA}$, and $a = 3 \text{ \AA}$.

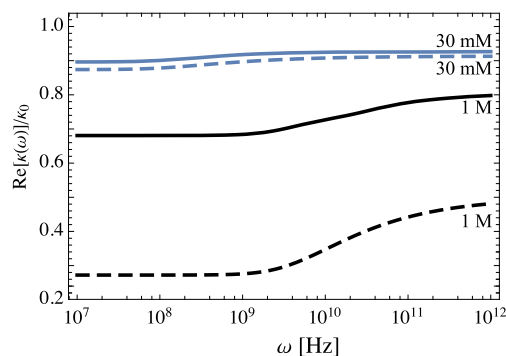


FIG. 4. Real part of the normalized conductivity rescaled by κ_0 for different concentration values as a function of the external field's oscillation frequency, ω . The normalized conductivity is plotted for the truncated potential (solid) and the Coulomb potential (dashed) for concentrations of 30 mM and 1M. The frequency value at which the conductivity transitions from a pseudo-plateau that equals the static conductivity to an increasing function scales roughly with n . Other parameter values are the same as for Fig. 3.

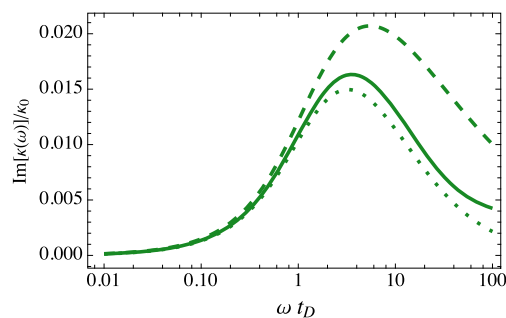


FIG. 5. Imaginary part of the normalized conductivity (rescaled by κ_0) for Coulomb potential (dashed line), truncated potential [solid line—Eq. (38)], and the soft-truncated potential [dotted line—Eq. (40)] for $n = 0.1\text{M}$. For high frequencies, $\omega \gg t_D^{-1}$ and low ones $\omega \ll t_D^{-1}$, the imaginary part is small, and the charge current is in phase with the external field. Other parameter values are the same as for Fig. 3.

The real part of the normalized conductivity is plotted in Fig. 4 for two very different concentration values, 30 mM and 1M, as a function of the driving oscillation frequency in Hz. At low frequencies, the conductivity behaves as the static one ($\omega = 0$), but as ω increases, the conductivity increases toward $\kappa = \kappa_0 + \kappa_{\text{hyd}}$, i.e., κ_{el} approaches zero. One can see that the frequency value at which this changeover occurs scales roughly with n . In other words, there is a critical frequency, $\omega_D = 1/t_D \sim n$, below which the conductivity behaves as the static conductivity.

In Fig. 5, the imaginary part of the normalized conductivity is plotted for the three interaction potentials. For pure Coulomb potential, the imaginary part accounting for the response phase-shift starts to decay at frequency $\omega t_D \approx 10$, while for the truncated and soft-truncated potentials, the decay begins at $\omega t_D \approx 2$. This leads to the conclusion that including the steric interactions in the interaction potential reduces the dephasing effect.

At high frequencies, compared to the ion or solvent inertial time t_1 defined earlier, the conductivity behavior changes significantly at the level of the Nernst-Einstein term. Such a behavior

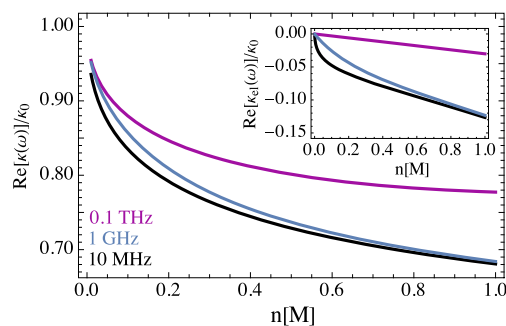


FIG. 6. Real part of the normalized conductivity as a function of the ion concentration for three driving frequencies, $\omega = 10$ MHz (black line), 1 GHz (blue line), and 0.1 THz (purple line), using the truncated potential. The blue curve for the intermediate frequency of 1 GHz crosses over between the static conductivity behavior at low frequencies (black line, $\omega = 10$ MHz) and the high-frequency conductivity behavior (purple line, $\omega = 0.1$ THz). The crossover is due to the dependence of the Debye time t_D on the concentration. Other parameter values are the same as for Fig. 3. The inset shows the rescaled electrostatic correction, κ_{el} [Eq. (38)], up to 1M for the same three frequencies as the main panel (κ_{hyd} is not shown as it does not depend on the frequency ω).

can be seen directly by examining an underdamped non-interacting electrolyte toy model, $m_{ion}\dot{\mathbf{v}}_{ion} + \mu^{-1}\mathbf{v}_{ion} = z_{\alpha}e\mathbf{E}_0g(t)$, where \mathbf{v}_{ion} is the ion velocity. These dynamics lead to a frequency dependence of the conductivity of inertial origin $\kappa_0(\omega) \sim \kappa_0/(1 + i\omega t_1)$. Our model, based on overdamped dynamics, cannot exhibit the latter.

Frequency dependence of the conductivity due to inertia is included in previous works.^{17,21} It can be analytically verified that for low frequencies (compared to t_1) and at low concentrations (the DH approximation), the prediction in Ref. 21 recovers that of Debye–Falkenhagen. However, the two theories strongly disagree at high frequencies due to inertia and memory effects.

It is worth mentioning that the theory in Ref. 21 does not produce closed-form expressions beyond the two limiting cases discussed earlier (low and high frequencies). In the intermediate regime, one has to solve the governing equations to evaluate the conductivity iteratively. Incorporating underdamped dynamics to account for the high-frequency effect into an SDFT model is left for future work.

Figure 6 presents the real part of the normalized conductivity as a function of the ion concentration at different driving frequencies, $\omega = 10$ kHz, 1 GHz, and 0.1 THz (using only the truncated potential). One can see a crossover between the static and high-frequency conductivity in the blue curve corresponding to the intermediate frequency, $\omega = 1$ GHz. The crossover is due to the dependence of the Debye time $t_D \sim 1/n$ on the concentration, leading to a change between static and high-frequency conductivity.

Our model is based on simple considerations that restrict it from describing all the rich phenomenology of electrolyte systems self-consistently; in particular, it assumes a constant dielectric susceptibility and viscosity. However, these quantities depend on the ionic concentration and the external field. Incorporating such refinements has been performed in Refs. 42 and 43.

Relation to experiments: The frequency-dependent conductivity was measured in some experiments.^{35,44–47} Unfortunately, there are specific difficulties in comparing our predictions with

experimental results. First, the dielectric susceptibility of water strongly decreases as a function of the dissolved salt concentration. This is the celebrated “dielectric decrement” phenomenon observed experimentally and discussed in Refs. 43 and 48–50.

In addition, the dielectric susceptibility decreases at high frequencies of the order of GHz.^{35,36,47} This effect alters the electrostatic interaction between the ions. Moreover, the increase in conductivity with the external field frequency happens at frequencies similar to the resonance frequency of water molecules. This leads to several complications with the measurements, including heating the aqueous solution.

Finally, in high-frequency experimental setups, boundary effects around the electrodes extend well into the electrolyte solution, making the measurement of bulk conductivity at high frequencies quite challenging.^{44,51} To our knowledge, the frequencies at which the conductivity was measured so far are lower than a few MHz. Up to these frequencies, the behavior is quasi-static; the conductivity does not depend on ω and is equal to its DC values. These observations make it hard to validate our predictions with relevant experimental data, although these predictions have the correct qualitative behavior as a function of salt concentration and driving frequency.

We also would like to comment on molecular-dynamic (MD) simulations that have been performed for similar frequency-dependent conductivity.^{17,36,52} To observe the Debye–Falkenhagen (DF) effect in an MD simulation, it is necessary to eliminate the dipolar effects of the solvent, as the change in the dielectric constant would mask the DF effect. A similar setting was investigated in Ref. 52. It was shown that the confinement (finite-size effect) significantly impacts the electrolyte dynamics. This renders the bulk behavior challenging to observe.

V. CONCLUSIONS

We calculated the frequency-dependent conductivity for binary monovalent electrolytes within the stochastic density functional theory (SDFT) framework. We examined several modified ion–ion interaction potentials to account for the short-range effect missing in the Debye–Falkenhagen (DF) theory that does not include the ion steric effect. By employing two modified Coulomb potentials that suppress unphysical, short-range electrostatic attraction, we demonstrate that the correction is relatively robust in terms of the details of the modified potential.

The DF effect is relatively small and, for various monovalent salts, falls in the same frequency range as water’s resonance frequency. This leads to a masking of the DF effect by the significant change in the relative dielectric constant. To adequately compare our findings to experiments, one would need to measure the conductivity of a 1:1 electrolyte in a solvent that does not present a strong frequency dependence of the dielectric constant in the GHz range. Alternatively, simulations that assume an implicit solvent may be used to avoid effects from the water molecules’ polarization.

The theory presented here can be generalized to multi-component electrolytes and multivalent ions. However, the latter is expected to limit the theory’s validity to lower concentrations due to strong electrostatic correlations and fluctuations,²⁶ which are not fully considered within our work.

SUPPLEMENTARY MATERIAL

In the [supplementary material 1](#), a video animation of the density–density correlation function $c_{+-}(x/\lambda_D, y/\lambda_D, t)$ over time is presented, where the lengths are measured in units of λ_D . The correlation c_{+-} is computed by taking numerically the Fourier transform of the solution in Eq. (32) for $g(t) = \cos(\omega_0 t)$. A pure Coulomb interaction potential is used. The three panels show a colormap of c_{+-} for different values of ω_0 . In order to enhance the deformation visibility, we set $\mathcal{E} = 3$. The arrows indicate the direction of the electric field. See [Fig. 2](#) for further details.

ACKNOWLEDGMENTS

The authors acknowledge I. Chikina, S. Nakamae, and A. Varlamov for their useful discussions of experimental works and B. Rotenberg, V. Démery, and P. Illien for comments and suggestions. D.A. acknowledges the NSFC-ISF Research Program, jointly funded by the National Science Foundation China (NSFC) and the Israel Science Foundation (ISF) under Grant No. 3396/19 and ISF Grant Nos. 213/19 and 226/24. Y.A. acknowledges support from the Kadanoff-Rice Postdoctoral Fellowship and the Zuckerman STEM Leadership Program.

AUTHOR DECLARATIONS

Conflict of Interest

The authors have no conflicts to disclose.

Author Contributions

Haggai Bonneau: Conceptualization (equal); Formal analysis (equal); Investigation (equal); Software (equal); Validation (equal); Visualization (equal); Writing – original draft (equal). **Yael Avni:** Conceptualization (equal); Formal analysis (equal); Investigation (equal); Validation (equal); Writing – review & editing (equal). **David Andelman:** Funding acquisition (equal); Methodology (equal); Supervision (equal); Writing – review & editing (equal). **Henri Orland:** Conceptualization (equal); Investigation (equal); Methodology (equal); Supervision (equal); Writing – review & editing (equal).

DATA AVAILABILITY

The data that support the findings of this study are available within the article.

REFERENCES

- J. Wilson, S. Shim, Y. Yu, A. Gupta, and H. Stone, *Langmuir* **36**, 7014 (2020).
- M. Bazant and T. Squires, *Curr. Opin. Colloid Interface Sci.* **15**, 203 (2010).
- M. Bazant, K. Thornton, and A. Ajdari, *Phys. Rev. E* **70**, 021506 (2004).
- S. Wall, *Curr. Opin. Colloid Interface Sci.* **15**, 119 (2010).
- P. Simon and Y. Gogotsi, *Nat. Mater.* **19**, 1151 (2020).
- P. Robin, N. Kavokine, and L. Bocquet, *Science* **373**, 687 (2021).
- M. McEldrew, Z. Goodwin, S. Bi, M. Bazant, and A. Kornyshev, *J. Chem. Phys.* **152**, 234503 (2020).
- S. Benaglia, M. Uhlig, J. Hernández-Muñoz, E. Chacón, P. Tarazona, and R. García, *Phys. Rev. Lett.* **127**, 196101 (2021).
- M. Gebbie, M. Valtiner, X. Banquy, E. Fox, W. Henderson, and J. Israelachvili, *Proc. Natl. Acad. Sci. U. S. A.* **110**, 9674 (2013).
- A. Smith, A. Lee, and S. Perkin, *J. Phys. Chem. Lett.* **7**, 2157 (2016).
- P. Debye and E. Hückel, *Phys. Z.* **24**, 305 (1923).
- L. Onsager, *Phys. Z.* **27**, 388 (1926).
- L. Onsager and S. Kim, *J. Phys. Chem.* **61**, 198 (1957).
- P. Debye and H. Falkenhagen, *Phys. Z.* **29**, 121 (1928).
- J. Anderson, *J. Non-Cryst. Solids* **172**, 1190 (1994).
- H. Falkenhagen, *Electrolytes* (Oxford University, Oxford, 1934), Chap. 9.
- A. Chandra, D. Wei, and G. Patey, *J. Chem. Phys.* **99**, 2083 (1993).
- C. Contreras Aburto and G. Nägele, *J. Chem. Phys.* **139**, 134109 (2013).
- C. C. Aburto and G. Nägele, *J. Chem. Phys.* **139**, 134110 (2013).
- A. Chandra and B. Bagchi, *J. Phys. Chem. B* **104**, 9067 (2000).
- A. Chandra and B. Bagchi, *J. Chem. Phys.* **112**, 1876 (2000).
- D. Dean, *J. Phys. A: Math. Gen.* **29**, L613 (1996).
- K. Kawasaki, *Physica A* **208**, 35 (1994).
- V. Démery and D. Dean, *J. Stat. Mech.: Theory Exp.* **2016**, 023106.
- J. Péraud, A. Nonaka, J. Bell, A. Donev, and A. Garcia, *Proc. Natl. Acad. Sci. U. S. A.* **114**, 10829 (2017).
- Y. Avni, D. Andelman, and H. Orland, *J. Chem. Phys.* **157**, 154502 (2022).
- Y. Avni, R. Adar, D. Andelman, and H. Orland, *Phys. Rev. Lett.* **128**, 098002 (2022).
- P. Robin, *J. Chem. Phys.* **160**, 060601 (2024).
- O. Bernard, M. Jardat, B. Rotenberg, and P. Illien, *J. Chem. Phys.* **159**, 164501 (2023).
- S. Mahdisoltani and R. Golestanian, *New J. Phys.* **23**, 073034 (2021).
- H. Bonneau, V. Démery, and E. Raphaël, *J. Stat. Mech.: Theory Exp.* **2023**, 073205.
- A. Donev, A. Garcia, J. Péraud, A. Nonaka, and J. Bell, *Curr. Opin. Electrochem.* **13**, 1 (2019).
- B. Øksendal, *Stochastic Differential Equations: An Introduction with Applications* (Springer, 2000).
- S. Kim and S. Karrila, *Microhydrodynamics: Principles and Selected Applications* (Butterworth-Heinemann, 2013).
- R. Buchner, G. Hefter, and P. May, *J. Phys. Chem. A* **103**, 1 (1999).
- G. Pireddu, C. Fairchild, S. Niblett, S. Cox, and B. Rotenberg, *Proc. Natl. Acad. Sci. U. S. A.* **121**, e2318157121 (2024).
- C. Gardiner, *Stochastic Methods* (Springer Berlin, 2009).
- R. Adar, S. Safran, H. Diamant, and D. Andelman, *Phys. Rev. E* **100**, 042615 (2019).
- C. Santangelo, *Phys. Rev. E* **73**, 041512 (2006).
- A. Lee, S. Kondrat, D. Vella, and A. Goriely, *Phys. Rev. Lett.* **115**, 106101 (2015).
- J. de Souza and M. Bazant, *J. Phys. Chem. C* **124**, 11414 (2020).
- H. Berthoumieux, V. Démery, and A. C. Maggs, *J. Chem. Phys.* **161**, 184504 (2024).
- D. Ben-Yaakov, D. Andelman, and R. Podgornik, *J. Chem. Phys.* **134**, 074705 (2011).
- I. Chikina, S. Nakamae, and A. Varlamov, *Colloids Interfaces* **7**, 58 (2023).
- N. Vinh, M. Sherwin, S. Allen, D. George, A. Rahmani, and K. Plaxco, *J. Chem. Phys.* **142**, 214501 (2015).
- M. Querry, R. Waring, W. Holland, G. Hale, and W. Nijm, *J. Opt. Soc. Am.* **62**, 849 (1972).
- A. Peyman, C. Gabriel, and E. Grant, *Bioelectromagnetics* **28**, 264 (2007).
- P. Biesheuvel, *Eur. Phys. J. E* **16**, 353 (2005).
- M. Hatlo, R. van Roij, and L. Lue, *Europhys. Lett.* **97**, 28010 (2012).
- J. López-García, J. Horno, and C. Grosse, *J. Colloid Interface Sci.* **428**, 308 (2014).
- I. Chikina and A. Varlamov, *Colloids Interfaces* **8**, 34 (2024).
- T. H. Ngoc Minh, G. Stoltz, and B. Rotenberg, *J. Chem. Phys.* **158**, 104103 (2023).